Plasmonic Terahertz Emitters and Detectors for Sensing and Wireless Communications

T. Otsuji[1], **A. Satou**[1], **S. Boubanga Tombet**[1], **T. Watanabe**[1], **G. Ducournau**[2], **Y. M. Meziani**[3], **W. Knap**[4], **and V. V. Popov**[5]

[1]Research Institute of Electrical Communication, Tohoku University, Sendai, Japan
[2]Institut d'Electronique, de Micro electronique et de Nanotechnologie
Universite de Lille, France
[3]Department de Fisca Aplicada, Universidad de Salamanca, Salamanca, Spain
[4]Laboratory Charles Coulomb & TERALAB
Université Montpellier 2 & CNRS, Montpellier, France
[5]Kotelnikov Institute of Radio Engineering and Electronics (Saratov Branch)
RAS, and Saratov State University, Saratov, Russia

Abstract— This paper reviews recent advances in emission and detection of terahertz (THz) radiation using two dimensional (2D) plasmons in semiconductor heterostructures and their applications. The device structure is based on a high-electron mobility transistor (HEMT) incorporating the asymmetrically interdigitated dual-grating gates (ADGGs). Its excellent THz emission and detection performances are experimentally demonstrated by using fabricated InP-based ADGG HEMTs. Their arrayed monolithic integration and module assembly/packaging issues are also discussed. Finally their applications to THz sensing and wireless communications are demonstrated.

1. INTRODUCTION

Realization of high power coherent terahertz (THz) emitters/oscillators and sensitive, high-speed THz detectors operating at room temperature are ones of the most challenging problems in THz applications, especially in THz wireless communications. Recently, THz emitters and detectors based on plasmons in two-dimensional (2D) electron channels, both of which were proposed by Dyakonov and Shur [1, 2], have made remarkable progress [3]. This paper reviews recent advances in emission and detection of THz radiation using two dimensional (2D) plasmons in semiconductor heterostructure integrated devices and their applications to sensing and high-speed wireless communication systems. The nonlinear dynamics of the 2D plasmons including the instability [1, 4] and rectification effects [2] is first presented as the operation principle of broadband intense emission and sensitive detection of THz radiation. Second, the device structure based on a high-electron mobility transistor (HEMT) incorporating the authors' original asymmetrically interdigitated dual-grating gates (ADGGs) is addressed [5, 6]. The superiority on instability (emissivity) and responsivity performances of the ADGG structure against the conventional symmetric DGG structure [7] is analytically manifested [5, 6]. Third, excellent terahertz emission [3, 8, 9] and detection [10–12] performances are experimentally demonstrated by using InP-based heterostructure material systems. Their arrayed monolithic integration and module assembly/packaging issues [13, 14] are also discussed. Finally their applications to terahertz-imaging-based sensing [9, 13–15] as well as high-speed wireless communications [16–18] are demonstrated.

2. THEORY

The 2D plasma wave is an in-plane collective charge-density wave. Its fluidic motions can be formulated by the hydrodynamic Euler equation and the continuity equation [1]. 2D electron channels in HEMTs consist of gated and ungated region (see Figure 1). The gated 2D plasmon receives transverse Coulomb force via gate capacitor which is far stronger than the in-plane force due to the geometrical situation so that it holds a linear dispersion. In a simple case of gradual-channel approximation with infinite channel width (perpendicular to the source-drain direction), the plasma-wave phase velocity s is given by $s = \sqrt{eV_0/m}$ where V_0 is the gate swing voltage. Assuming $V_0 = O[1\,\mathrm{V}]$ and $m = O[0.1m_0]$ (m_0 is the electron rest mass in vacuum) for InP-based heterostructure HEMTs, s becomes $O[1 \times 10^6\,\mathrm{m/s}]$ which is at least two orders of magnitude higher than the electron drift velocity of any compound semiconductors. When we consider a sub-micrometer gate-length HEMT, the fundamental mode of gated 2D plasmons stays at frequency in the THz range. This is the main advantage for use in plasmon resonant modes that can operate in the frequencies far beyond the transit frequency limit of transistors.

Coherent plasmonic THz emission is realized by the plasma wave instabilities described by the Dyakonov-Shur (DS) Doppler-shift model [1] and/or Ryzhii-Satou-Shur (RSS) transit-time model [4]. When a single-gate HEMT is situated in source-terminated and drain-opened configuration with dc potential at drain terminal with respect to the source terminal, the drain end of the channel becomes depleted so that the drain-side impedance is mainly given by the depletion capacitance and takes a high value at high frequencies. In such a case, the reciprocal Doppler-shifting plasma waves reflecting at an asymmetric drain-opened boundary promote the increments of their intensity leading to self-oscillation of instability [1]. The plasma-wave increment is a dimensionless parameter in which the imaginary part of angular frequency is normalized to the fundamental resonant frequency. Figure 1(b) shows a calculated result for the plasma instability increment versus the ratio of the electron drift velocity to the plasma velocity for a 32-nm gate InP-based HEMT [3]. The positive values of the increment give rise to instability in an idealistic loss-less case. In reality with plasma damping caused by scattering, the Drude loss factor should consider to obtain an overall gain, which is shown as a threshold level.

At large drain-source voltages, the THz conductivity of the high-field gate-drain region in a HEMT is not so small due to relatively high electron drift velocity v_{gd}. In this case v_{gd} becomes much higher than that in the intrinsic channel region v_d. As a result the ac current is induced in the gated channel. Its frequency dependence is directly reflected by the electron transit time τ_{dd} at the gate-drain region $\tau_{gd} = L_d/v_{gd}$ where L_d is the length of the gate-drain region, promoting the RSS instability [4]. Figure 1(c) plots the calculated DS and RSS instability indices γ_{DS} and γ_{RSS} as functions of the gate length L_g and the fundamental plasmon frequency.

Hydrodynamic Euler equation includes a quadratic term in a product of the local carrier velocity and its spatial gradient. The continuity equation includes the other quadratic term in a product of the local carrier velocity and the local carrier density. These terms give rise to nonlinear convective and conductive rectification effects to the electromagnetic radiation, respectively. The former is called as the plasmonic 'ratchet' effect and has a Drude-type monotonic frequency dependence whereas the latter is called as the plasmonic 'drag' effect and has a frequency-independent response [5, 11].

When the plasmon cavity length (corresponding to the intrinsic gate length) is shorter (longer) than the coherent length given by the product of the plasmon velocity and the momentum relaxation time, the rectified photoresponse becomes resonant-like (non-resonant-like). It is noted that even for the non-resonant, over-damped cases, rectified component is "non-zero," due to the aforementioned plasmon nonlinearities [19]. In general at room temperature the gate length of the order of sub micrometers is longer than the coherent length in III-V or group-IV semiconductors, which in turns resulting in non-resonant THz detection at room temperature. The responsivity of the non-resonant detection is analytically derived from the current-voltage characteristics of the HEMT operation, which is proportional to the transconductance, inverse conductivity, and square of the radiation intensity [20]. Thus, in general, the responsivity takes a maxima at a gate swing voltage close to the threshold level [20]

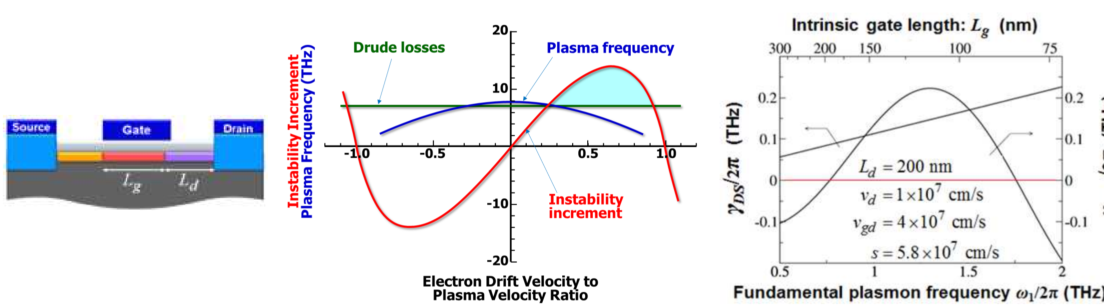

(a) (b) (c)

Figure 1: (a) Schematics cross sectional view of a HEMT. (b) Increment of DS instability as a function of the ratio of the electron drift velocity to the plasma velocity [3]. (c) Calculated DS and RSS instability indices γ_{DS} and γ_{RSS} as functions of the intrinsic gate length L_g and the fundamental plasmon frequency [4]. Positive values correspond to the instable cases.

3. ADGG HEMT EMITTERS AND DETECTORS

In order to realize intense coherent monochromatic THz emission and highly sensitive THz detection we introduced our original ADGG structure (Figure 2) [4]. In the ADGG structure the DGG is implemented with asymmetric inter-finger spaces. THz electric field distribution and resultant photoresponse were numerically simulated using a self-consistent electromagnetic approach combined with the perturbation theory for the hydrodynamic equations for 2D plasmons in HEMTs under periodic electron density modulation conditions [5]. Figure 3(a) shows giant enhancement of the responsivity (by four orders of magnitude) in an ADGG HEMT under drain-unbiased conditions. When the ADGG HEMT is dc-drain biased, the asymmetry of the plasmonic cavity is enhanced enormously as shown in Figure 3(b), resulting in further enhancement of the responsivity by orders of magnitude. It is reasonable to suggest that similar enhancement should be also exhibited for the DS and RSS instabilities in the ADGG HEMT. We modeled the plasmon instabilities based on Boltzmann transport equation and self-consistent Poisson's equation. Figure 3(c) plots the DS and RSS growth rates for a typical case of structural and material parameters, exhibiting peaks in shorter L_{g1} caused by the RSS instability and a flat response caused by the DS instability.

The ADGG HEMTs were designed and fabricated using InAlAs/InGaAs/InP materials (see Figure 1) [5]. Asymmetric factor, the ratio of the inter-finger spaces, d_1/d_2, was fixed to be 0.5. The grating gates G1 with narrower fingers L_{g1}, serving plasmon cavity gates, were designed to be chirped ranging from 215 to 430 nm.

After processing the ADGG HEMT, a vertical photonic cavity with a high finess of ~ 60 was formed (see Figure 1).

First, we observed the THz emission from the device using a Fourie-transform spectrometer wish a 4.2-K Si bolometer. As seen in Figure 4(a) intense emission of Fabry-Perot modes with a sharp linewidth $\sim 1.23\,\mathrm{cm}^{-1}$ (~ 37 GHz) was observed at room temperature (290 K). As a bias dependence, by increasing V_{ds} the whole emission intensity of Fabry-Perot modes raises, reflecting the hot-plasmon-originated broadband background emission. Furthermore, by applying appropriate biases for DGG: V_{g1} of 0 V and V_{g2} of -0.55 V to make a strong contrast on the electron densities on plasmonic cavities the peak at ~ 3.55 THz was enhanced, reflecting the 3rd harmonics of the plasmon resonance driven by the DS instability. At lower temperatures electron momen-

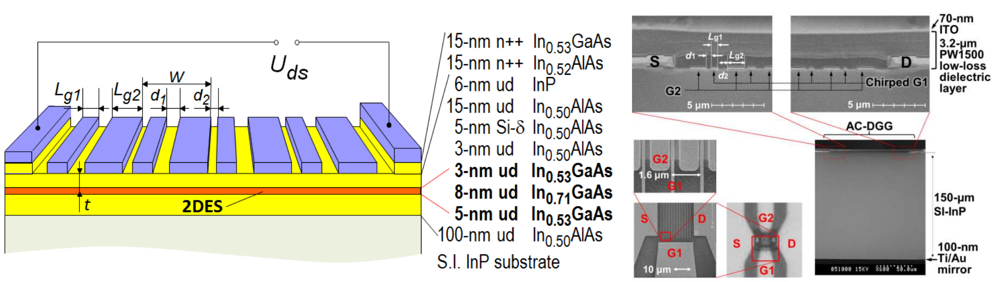

Figure 2: Schematic view and scanning electron micrographic images of an AC-DGG HEMT THz emitter/detector.

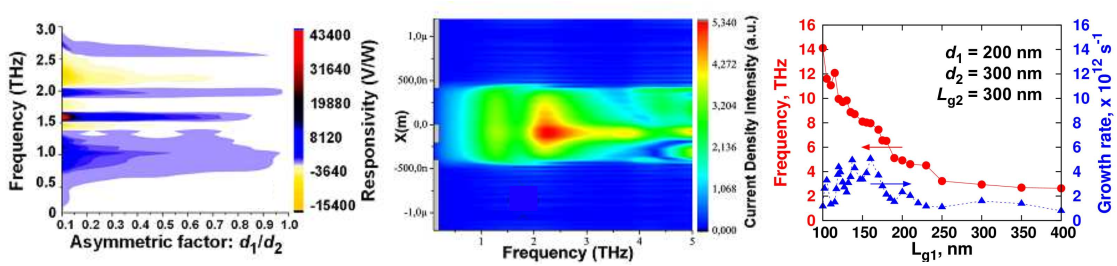

(a) (b) (c)

Figure 3: (a) Simulated relative responsivity as a function of d_1/d_2. $L_{g1} = 400$ nm, $L_{g2} = 2.4$ μm, $d_1 + d_2 = 800$ nm, $W = 3.6$ μm. Electron density under G2: $2.5 \times 10^{11}\,\mathrm{cm}^{-2}$, and that the other area: $2.5 \times 10^{12}\,\mathrm{cm}^{-2}$. (b) Simulated current distribution underneath a unit ADGG cell for the asymetric factor of $d_1/d_2 = 0.5$. (c) Simulated growth rate vs. L_{g1}. $d_1 = 200$ nm, $d_2 = 300$ nm, $L_{g1} = 300$ nm.

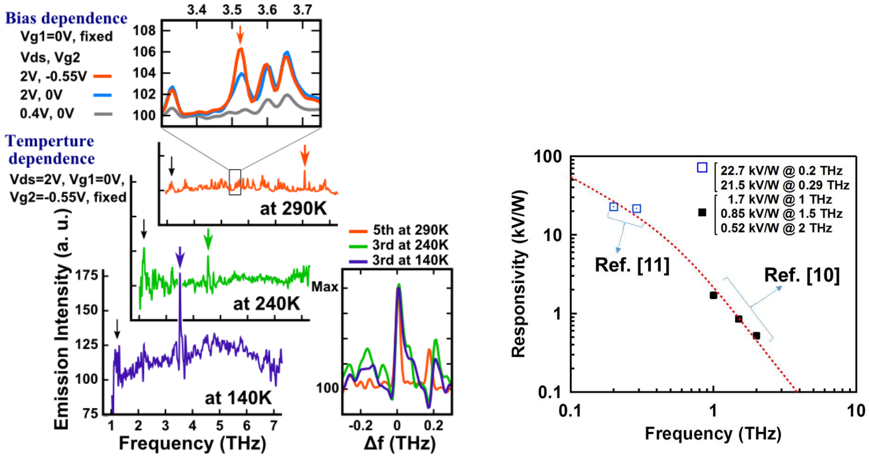

(a) (b)

Figure 4: (a) Bias and temperature dependences of emission spectra for the fabricated ADGG HEMT [3]. (b) Frequency dependence of the responsivity obtained experimentally (filled circles and squares) and theoretical fitting (dashed line) [11].

tum relaxation times increase and hot-plasmon background is suppressed, resulting in more intense monochromatic coherent emission at ~ 3.55 THz corresponding to the 3rd plasmon mode matched to a Fabry-Perot mode at 140 K.

Second, we measured the photovoltage of the ADGG HEMT samples upon input THz waves at normal incidence, with polarization parallel to the source-to-drain direction at 300K under zero drain-to-source bias conditions. Measured responsivity is plotted in Figure 4(b), demonstrating the record detection responsivity of 22.7 kV/W (2.2 kV/W) at 200 GHz (1 THz) at 300 K with low noise equivalent power of 0.48 pW/Hz$^{0.5}$ (15 pW/Hz$^{0.5}$) [10, 11]. The frequency dependence of the responsivity agrees well with the theoretical model, showing the plasmon drag effect predominant at relatively low frequencies and the plasmon ratchet effect predominant at relatively high frequencies [11]. When drain-source is dc biased in the subthreshold region, the responsivity increases by one order of magnitude from the level under unbiased conditions while suppressing the increase in the noise figure [12].

4. FUTURE DIRECTIONS

4.1. Arrayed Integration

One critical issue of the A-DGG HEMT is a mismatch of the device active area ($< 20 \times 20\,\mu\text{m}^2$) and the spot size of the THz beam, which is on the order of its wavelength ($> 300\,\mu$m). It causes inefficient coupling of the total incoming/outgoing THz wave to/from the device and, in turn, results in inefficient external performances, despite the portion of the incoming/outgoing THz wave within the active area is effectively coupled to the devices. The active area is limited mainly by the technological difficulty to make interdigitated dual-grating gates with submicron lengths (and with widths several orders of magnitude larger) over tens of periods. A natural solution for this is 2D-arrayed integration of emitters/detectors. The series connection of detectors in an array should result in the summation of photovoltage of each detector, and the total photovoltage should become the photovoltage of a single detector multiplied by the number of the detectors, at the best. For an emitter array, the variation of emission frequency (and the phase) of each emitter may degrade the total output power from the ideal summation of emission power of each emitter. The mutual injection locking among emitters, however, is expected to be manifested due to the strong nonlinearity of plasmons, leading to a monochromatic coherent emission from the array.

As a first step towards the monolithic integration of the 2D-arrayed emitters/detectors, we measured the photovoltage of an array of 1×4 A-DGG detectors (Figure 5(a)), where source and drain contacts of the detectors laid on a die are connected in series by wire bonding. Figure 5(b) shows the external responsivity of the detector array at 0.8 THz as well as that of a single detector with the same design and the same bias conditions. Here, the external responsivity refers to the responsivity normalized by the total input power. As shown in Figure 5(b), the responsivity is almost 4 times larger for the detector array than the single detector as expected. This result clearly

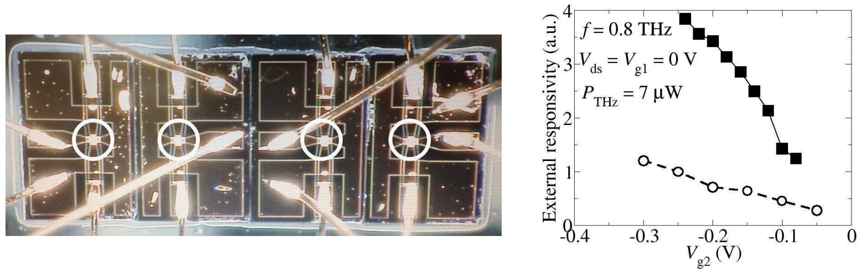

(a) (b)

Figure 5: (a) Array of 1×4 A-DGG detectors. Device active areas are indicated inside white circles. (b) External responsivity of the detector array (filled squares) compared with that of a single detector (opaque circles).

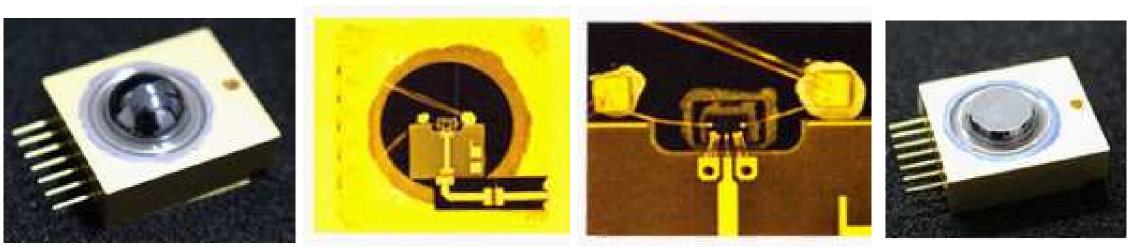

(a) (b) (c) (d)

Figure 6: (a) Image of a single detector module. (b) Detector and a waveguide mounted on the back of the Si-lens inside the module. (c) Closer view of the mounted detector. (d) Image of an arrayed detector module.

demonstrates the effectiveness of the arrayed integration. Much denser detector array ($> 10 \times 10$ in total active area with $< 1 \times 1\,\text{mm}^2$ is possible) is thus expected to be very effective to maximize the external performance.

4.2. Packaging

To build up imaging or wireless communication systems with A-DGG emitters/detectors, packaging them into an assembled module is inevitable. Here, we developed such modules dedicated for single and arrayed emitters/detectors. For a single emitter/detector, we developed a module with a semispherical Si lens where the device is mounted onto the back surface of the lens at the focal point (see Figures 6(a)–(c)). In addition, the output port for the detector (i.e., drain contact) is connected to a coplanar waveguide and then to an RF connector embedded into the module. These enable the transmission of received signal with modulation speed up to 40 GHz. For an emitter/detector array designed to mount 3×2 devices, on the other hand, a flat Si window is adapted because the sizes of the arrays are larger than the spot size of the THz beam at the focal point (see Figure 6(d))

There is a room for further improvement on module assembly and packaging. First, the output port of the detector and the input port of the emitter for modulation signal must be impedance-matched to $50\,\Omega$. Second, embedding a low-noise amplifier to the detector module is an effective way to improve the responsivity. Third, the lens shape must be optimized depending on the total active area of a single device or an array as well as on the directivity of emitters Those are necessary to exploit ultimate performance of A-DGG emitters/detectors.

4.3. Applications

THz imaging is successfully performed utilizing the ADGG HEMTs as is demonstrated in Refs. [9, 15]. Our interest is now much directed to the application of the ADGG HEMT detectors to the sub-THz wireless communication. The standard single-gate HEMT was successfully utilized for detection of sub-THz wireless transmission data traveled over a 1-m distance on a 300-GHz carrier [16–18]. The results suggests that the extension of the transmission distance by orders of magnitude (from the order of "meter" to "kilometer") could be feasible by replacing the single-chip single-gate HEMT detector chip to a 2D-arrayed ADGG HEMT detector module.

5. CONCLUSIONS

Recent advances in emission and detection of terahertz radiation using 2D plasmons in semiconductor heterostructure integrated devices and their applications to sensing and high-speed wireless communication systems were reviewed. The Doppler-shift effect of the plasma wave velocity under an asymmetric plasmon cavity boundary and/or the spatial modulation of electron transit time in a sub-micrometer scaled 2D plasmon system with a non-uniform 2D electron density distribution can promote the plasmon instability, resulting in self-oscillation of plasmons in the terahertz regime. The hydrodynamic nonlinearity of 2D plasmons can rectify the incoming electromagnetic radiation, resulting in photovoltaic detection of terahertz radiation under an asymmetric 2D plasmon cavity boundary. The device structure that can provide practical emission and detection performances were addressed, which is based on a high-electron mobility transistor and incorporates the authors' original ADGGs. Numerical analysis revealed that in comparison with conventional symmetric DGG structure the asymmetric DGG can substantially improve the detection sensitivity as well as the instability (emissivity) by three to four orders of magnitude. Excellent terahertz emission and detection performances including coherent, monochromatic emission beyond 1-THz range at relatively low temperatures and the record detection responsivity of 22.7 kV/W (2.2 kV/W) at 200 GHz (1 THz) at 300 K with low noise equivalent power of 0.48 $pW/Hz^{0.5}$ (15 $pW/Hz^{0.5}$) were experimentally demonstrated by using InAlAs/InGaAs/InP heterostructure material systems. The frequency dependence of the responsivity was in good agreement with the theory deduced from the plasmonic drag and ratchet effects. Their arrayed monolithic integration and module assembly/packaging issues were also addressed. Their applications to terahertz-imaging-based sensing as well as high-speed wireless communications were demonstrated.

ACKNOWLEDGMENT

The authors acknowledge Drs. Y. Takida, H. Ito, and H. Minamide at RIKEN Sendai, Japan, and Dr. D. Coquillat at LC2-Lab., CNRS-Montpellier-II, France for their contributions on the detection measurement and for fruitful discussion about the result. A.S. and T.O. thank NTT-AT Corp. for the cooperation in processing sample fabrication and NTT Electronics Corp. for the cooperation in module assembly and packaging. This work is financially supported in part by JST-ANR, Japan and France, and SCOPE (#145002001), MIAC, Japan. VVP acknowledges the support from RFBR (##13-02-12070, 14-02-92102, and 15-02-02989), Russia

REFERENCES

1. Dyakonov, M. and M. Shur, "Shallow water analogy for a ballistic field effect transistor: New mechanism of plasma wave generation by dc current," *Phys. Rev. Lett.*, Vol. 71, 2465–2468, 1993.
2. Dyakonov, M. and M. Shur, "Detection, mixing, and frequency multiplication of terahertz radiation by two-dimensional electronic fluid," *IEEE Trans. Electron. Dev.*, Vol. 43, 1640–1645, 1996.
3. Otsuji, T. and M. S. Shur, "Terahertz plasmonics: Good results and great expectations," *IEEE Microwave Magazine*, Vol. 15, 43–50, 2014.
4. Ryzhii, V., A. Satou, and M. Shur, "Plasma Instability and Terahertz generation in HEMTs due to electron transit-time effect," *IEICE Trans. Electron.*, Vol. E89-C, 1012, 2006.
5. Popov, V. V., D. V. Fateev, T. Otsuji, Y. M. Meziani, D. Coquillat, and W. Knap, "Plasmonic terahertz detection by a double-grating-gate field-effect transistor structure with an asymmetric unit cell," *Appl. Phys. Lett.*, Vol. 99, 243504, 2011.
6. Otsuji, T., T. Watanabe, S. A. Boubanga Tombet, A. Satou, V. Ryzhii, V. Popov, and W. Knap, "Emission and detection of terahertz radiation using two dimensional plasmons in semiconductor nano-heterostructures for nondestructive evaluations," *Opt. Eng.*, Vol. 53, 031206, 2013.
7. Otsuji, T., M. Hanabe, T. Nishimura, and E. Sano, "A grating-bicoupled plasma-wave photomixer with resonant-cavity enhanced structure," *Opt. Express*, Vol. 14, 4815–4825, 2006.
8. Watanabe, T., Y. Kurita, A. Satou, T. Suemitsu, W. Knap, V. V. Popov, and T. Otsuji, "Plasmonic terahertz monochromatic coherent emission from an asymmetric chirped dual-grating-gate InP-HEMT with a photonic vertical cavity," *Device Research Conference (DRC), 2013 71st Annual*, 129–130, Notre Dame, IN, USA, June 24, 2013.

9. Otsuji, T., T. Watanabe, S. Boubanga Tombet, A. Satou, W. Knap, V. Popov, M. Ryzhii, and V. Ryzhii, "Emission and detection of terahertz radiation using two-dimensional electrons in III-V semiconductors and graphene," *IEEE Trans. Terahertz Sci. Technol.*, Vol. 3, 63–72, 2013.
10. Watanabe, T., S. Boubanga Tombet, Y. Tanimoto, D. Fateev, V. Popov, D. Coquillat, W. Knap, Y. Meziani, Y. Wang, H. Minamide, H. Ito, and T. Otsuji, "Ultrahigh sensitive plasmonic terahertz detector based on an asymmetric dual-grating gate HEMT structure," *Solid State Electron.*, Vol. 78, 109–114, 2012.
11. Kurita, Y., G. Ducournau, D. Coquillat, A. Satou, K. Kobayashi, S. Boubanga Tombet, Y. M. Meziani, V. V. Popov, W. Knap, T. Suemitsu, and T. Otsuji, "Ultrahigh sensitive sub-terahertz detection by InP-based asymmetric dual-grating-gate high-electron-mobility transistors and their broadband characteristics," *Appl. Phys. Lett.*, Vol. 104, 251114, 2014.
12. Boubanga-Tombet, S., Y. Tanimoto, A. Satou, T. Suemitsu, Y. Wang, H. Minamide, H. Ito, D. V. Fateev, V. V. Popov, and T. Otsuji, "Current-driven detection of terahertz radiation using a dual-grating-gate plasmonic detector," *Appl. Phys. Lett.*, Vol. 104, 262104, 2014.
13. Tsuda, Y., T. Komori, A. El Fatimy, T. Suemitsu, and T. Otsuji, "Application of plasmonic microchip emitters to broadband terahertz spectroscopic measurement," *J. Opt. Soc. Am. B*, Vol. 26, A52–A57, 2009.
14. Schuster, F., D. Coquillat, H. Videlier, M. Sakowicz, F. Teppe, L. Dussopt, B. Giffard, T. Skotnicki, and W. Knap, "Broadband terahertz imaging with highly sensitive silicon CMOS detectors," *Opt. Express*, Vol. 19, 7827–7832, 2011.
15. Watanabe, T., S. Boubanga Tombet, Y. Tanimoto, D. Fateev, V. Popov, D. Coquillat, W. Knap, Y. Meziani, Y. Wang, H. Minamide, H. Ito, and T. Otsuji, "InP-and GaAs-based plasmonic high-electron-mobility transistors for room-temperature ultrahigh-sensitive terahertz sensing and imaging," *IEEE Sensors J.*, Vol. 13, 89–99, 2013.
16. Blin, S., F. Teppe, L. Tohme, S. Hisatake, K. Arakawa, P. Nouvel, D. Coquillat, A. Penarier, J. Torres, L. Varani, W. Knap, and T. Nagatsuma, "Plasma-wave detectors for terahertz wireless communication," *IEEE Electron Dev. Lett.*, Vol. 33, 1354–1356, 2012.
17. Blin, S., L. Tohme, D. Coquillat, S. Horiguchi, Y. Minamikata, S. Hisatake, P. Nouvel, T. Cohen, A. Penarier, F. Cano, L. Varani, W. Knap, and T. Nagatsuma, "Wireless Communication at 310 GHz using GaAs high-electron-mobility transistors for detection," *J. Comm. Networks*, Vol. 15, 559–568, 2013.
18. Tohmé, L., S. Blin, G. Ducournau, P. Nouvel, D. Coquillat, S. Hisatake, T. Nagatsuma, A. Pénarier, L. Varani, W. Knap, and J.-F. Lampin, "Terahertz wireless communication using GaAs transistors as detectors," *Electron. Lett.*, Vol. 50, 323–325, 2014.
19. Knap, W., M. Dyakonov, D. Coquillat, F. Teppe, N. Dyakonova, J. Lusakowski, K. Karpierz, M. Sakowicz, G. Valusis, D. Seliuta, I. Kasalynas, A. El Fatimy, Y. M. Meziani, and T. Otsuji, "Field effect transistors for terahertz detection: Physics and first imaging applications," *J. Infrared Milli. Terahz Waves*, Vol. 30, 1319–1337, 2009.
20. Sakowicz, M., M. B. Lifshits, O. A. Klimenko, F. Schuster, D. Coquillat, F. Teppe, and W. Knap, "Terahertz responsivity of field effect transistors versus their static channel conductivity and loading effects," *J. Appl. Phys.*, Vol. 110, 054512, 2011.